

Thermal buckling of porous FGM plate integrated surface-bonded piezoelectric

Mokhtar Ellali¹, Khaled Amara² and Mokhtar Bouazza^{*3,4}

¹Smart Structures Laboratory, University of Ain Témouchent-Belhadj Bouchaib, 46000, Algeria

²Department of Civil Engineering, University of Ain Témouchent-Belhadj Bouchaib, 46000, Algeria

³Department of Civil Engineering, University Tahri Mohamed of Bechar, Bechar 08000, Algeria

⁴Laboratory of Materials and Hydrology (LMH), University of Sidi Bel Abbes, Sidi Bel Abbes 22000, Algeria

(Received July 3, 2023, Revised December 8, 2023, Accepted January 12, 2024)

Abstract. In the present paper, thermal buckling characteristics of functionally graded rectangular plates made of porous material that are integrated with surface-bonded piezoelectric actuators subjected to the combined action of thermal load and constant applied actuator voltage are investigated by utilizing a Navier solution method. The uniform temperature rise loading is considered. Thermomechanical material properties of FGM plates are assumed to be temperature independent and supposed to vary through thickness direction of the constituents according to power-law distribution (P-FGM) which is modified to approximate the porous material properties with even and uneven distributions of porosities phases. The governing differential equations of stability for the piezoelectric FGM plate are derived based on higher order shear deformation plate theory. Influences of several important parameters on the critical thermal buckling temperature are investigated and discussed in detail.

Keywords: functionally graded materials; higher order shear deformation plate theory; piezoelectric; porosities; Thermal buckling

1. Introduction

Plate-type structural components are extensively used in majority of the engineering structures, among them, those employed in aerospace, naval, power plant, mechanical, civil, and ground vehicle structures. Due to the optimization targets frequently considered in these components, to minimize the costs, weights, fuel consumption, etc., these components maybe vulnerable to sever in-plane loads (e.g., compression, shear, thermal, or a combination of them). Therefore, reliability of design of such components requires carefully evaluating the buckling loads which can heavily limit the allowable bearing capacity. Therefore, it is important to study the buckling and postbuckling behaviors of plates under mechanical, thermal and combined thermomechanical loads for accurate and reliable design. Some works about the stability of plate relating to present study are introduced in the following. For examples, For examples, Reddy (2004), Boley and Weiner (1960), Chen *et al.* (1991), Ganapathi and Touratier (1997), Bouazza *et al.* (2013, 2017,

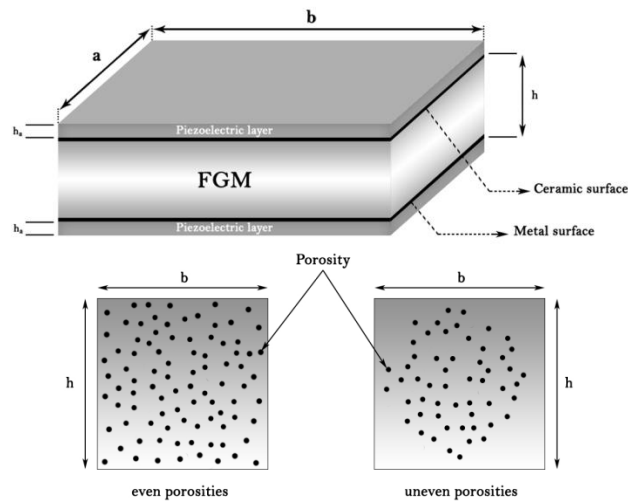
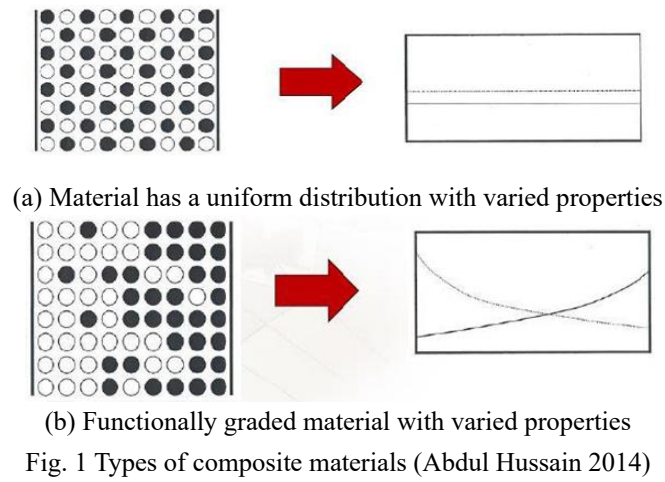
*Corresponding author, Professor, E-mail: bouazza_mokhtar@yahoo.fr, bouazza.mokhtar@univ-bechar.dz

2023), Becheri *et al.* (2016). Influence of temperature on the beams behavior strengthened by bonded composite plates studied by Bouazza *et al.* (2019).

The use of smart materials, as sensors and actuators, for the control of the mechanical behavior of smart structural systems, is becoming more prevalent. Some examples of the smart materials deployed include piezoelectrics, shape memory alloys and rheological-fluids (Liew *et al.* 2003). Piezoelectric materials are materials that convert electrical current to mechanical force and vice versa. Hence, piezoelectric materials are extensively used in sensors and actuators. Because of high stress concentrations, laminated piezoelectric materials delaminate and fail. Therefore, it was proposed to fabricate a new form of piezoelectric materials with functionally graded distribution of material properties which are called functionally graded piezoelectric materials (FGPMs) (Jam and Nia 2012). Due to the importance and wide engineering applications of piezoelectric FGMs, the behavior of these materials has been addressed by many investigators. For example, Liew *et al.* (2003), Mirzavand and Eslami (2011), Arefi and Rahimi (2012), Nami *et al.* (2015), Ghasemabadian and Kadkhodayan (2016), Amara *et al.* (2016).

Recently, Ghasemabadian and Kadkhodayan (2016), Investigated of buckling behavior of functionally graded piezoelectric rectangular plates under open and closed circuit conditions. Bimorph piezoelectric energy harvester structurally integrated on a trapezoidal plate presented by Avsar and Sahin (2016). Krommer *et al.* (2016) studied the nonlinear buckling and post-buckling behaviour of thin piezoelectric plates. Xiong and Tian (2017) studied the thermo-piezo-elastic of FGM piezoelectric plate under thermal shock. Buckling analysis of piezoelectric coupled transversely isotropic rectangular plates is investigated by Ghasemabadian and Saidi (2017) using the first-order shear deformation plate theory. In order to overcome the limitations of traditional methods, at recent years the novel and modified methods have been proposed for investigation of flexural and buckling behavior of the composite plates (Ellali *et al.* 2022, 2024, Nazira *et al.* 2019, Ebrahimi *et al.* 2019, Kar *et al.* 2015, 2016, 2017, Rathore *et al.* 2015, Shyam *et al.* 2023). Guessas *et al.* (2018) investigated the effect of porosity on the buckling behavior of carbon nanotube-reinforced composite porous plates using analytical method. Two types of distributions of uniaxially aligned reinforcement material are utilized which uniformly (UD-CNT) and functionally graded of plates (FG-CNT). Surface and flexoelectricity effects on size-dependent thermal stability analysis of smart piezoelectric nanoplates presented by Ebrahimi and Barati (2018). Ellali *et al.* (2018) investigated mechanical buckling analysis of magneto-electroelastic plate resting on Pasternak foundation is based on the third-order shear deformation plate theory. Karami *et al.* (2018) studied thermal buckling of embedded sandwich piezoelectric nanoplates with functionally graded core via a nonlocal second-order shear deformation formulation.

This paper focuses on the thermal buckling of porous functionally graded rectangular plates that are integrated with surface-bonded piezoelectric actuators subjected to the combined action of thermal loading and constant applied actuator voltage with two different porosity distributions in part of FGM. These types of porosity distributions, namely, even and uneven, through the thickness directions are considered. The uniform thermal loading is considered. An analytical solution is obtained for porous piezoelectric FGM plates with simple support via higher order shear deformation plate theory. The material properties are assumed temperature independent and vary continuously through the thickness direction according to modified power-law form. The derived equilibrium and buckling equations are then solved analytically for a plate with simply supported boundary conditions. These equations are solved by using Navier type method.



2. Theoretical formulation

Functionally graded materials are composite materials, macroscopically heterogeneous, with mechanical properties that vary continuously from one surface to another (Fig. 1). This continuous change which leads to graded properties in this type of materials, caused by a function of position of chemical composition, microstructure or atomic order.

2.1 Effective material properties of FGM plates with porosity distributions and integrated two perfectly bonded identical piezoelectric layers

Consider an functionally graded rectangular plate with porosities and integrated two perfectly bonded identical piezoelectric layers at the top and bottom surfaces as shown in Fig. 2. The width,

length and thickness of the FGM plate are represented by b , a and $2h$, respectively. In addition, h_a denotes the thickness of the each piezoelectric layer and the total thickness of the structure is also represented by t in which $t = 2(h + h_a)$

The effective material properties of FGM plates with two kinds of porosity distributions which are distributed identically in two phases of ceramic and metal can be expressed by using the modified rule of mixture as (Wattanasakulpong and Ungbhakorn 2014)

$$P = P_c \left(V_c - \frac{e}{2} \right) + P_m \left(V_m - \frac{e}{2} \right) \quad (1)$$

Where, e is the volume fraction of porosities ($e \ll 1$), for perfect FGM, e is set to zero, P_c and P_m are the material properties of ceramic and metal, and V_c , V_m are the volume fraction of ceramic and metal, respectively; the compositions are represented in relation to

$$V_c + V_m = 1 \quad (2)$$

Then, the volume fraction of ceramic V_c can be written as follows

$$V_c = \left(\frac{z}{h} + \frac{1}{2} \right)^k \quad (3)$$

Here, z is the distance from the mid-plane of the FGM plate and k is power law exponent the nonnegative variable parameter ($k \geq 0$) which determines the material distribution through the thickness of the plates. According to this distribution, we have a fully metal plate for large values of k and fully ceramic plate remains when $k = 0$. In this paper, imperfect FGM has been studied with two types of porosity distributions (even and uneven) across the plate thickness due to defect during fabrication.

For the even distribution of porosities (FGM-I), the effective material properties are obtained as follows

$$P(z) = (P_c - P_m)V_c + P_m - \frac{e}{2}(P_c + P_m) \quad (4)$$

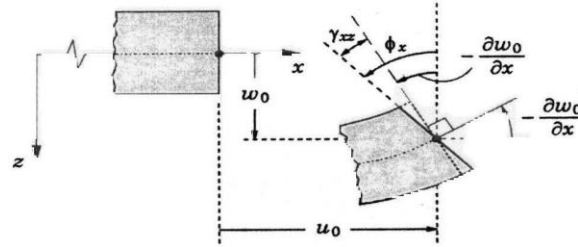
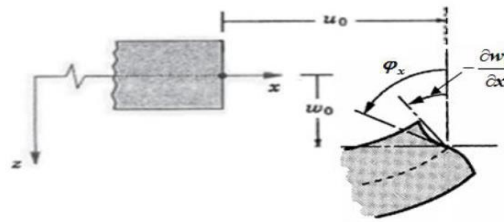
where the subscripts of m, c denote the metal and ceramic constituents. For the second type, uneven distribution of porosities (defined as FGM-II) the effective material properties are replaced by the following form

$$P(z) = (P_c - P_m)V_c + P_m - \frac{e}{2}(P_c + P_m) \left(1 - \frac{2|z|}{h} \right) \quad (5)$$

Here, it should be noted that the FGM-I has porosity phases with even distribution of volume fraction over the cross section, while the FGM-II has porosity phases spreading frequently nearby the middle zone of the cross section and the amount of porosity seems to be linearly decreased to zero at the top and bottom of the cross section.

2.2 Displacement field and strains

The classic Reissner-Mindlin model (FSDT, First order Shear Deformation Theory) introduces the effect of transverse shear, the kinematic hypothesis Bouazza (2017) is adopted: the normal remains straight but not perpendicular to the average surface (because of the effect of transverse shear) in the deformed configuration (Fig. 3). while the higher order theory model was proposed is


 Fig. 3 Kinematics of first order shear deformation theory (Nguyen *et al.* 2014)

 Fig. 4 Kinematics of higher order theory (Nguyen *et al.* 2014)

based on a nonlinear distribution of displacement fields following thickness. (Fig. 4).

The third-order plate theory of Reddy (2004) is based on the displacement field

$$\begin{aligned} u_1(x, y, z) &= u_0(x, y) + z\varphi_x(x, y) - c_1 z^3 \left(\varphi_x + \frac{\partial w_0}{\partial x} \right) \\ u_2(x, y, z) &= v_0(x, y) + z\varphi_y(x, y) - c_1 z^3 \left(\varphi_y + \frac{\partial w_0}{\partial y} \right) \\ u_3(x, y, z) &= w_0(x, y) \end{aligned} \quad (6)$$

Where (u_0, v_0, w_0) and (φ_x, φ_y) have the same physical meaning as in the first-order theory; they denote the displacements and rotations of transverse normals on the plane $z = 0$, respectively. Then the displacement field of FSDT is obtained by setting $c_1 = 0$, and for the Reddy third-order theory, it is equal to $c_1 = 4/3h^2$.

The von Kármán non-linear strains of TSDT which account for small strains and moderate rotations are

$$\begin{aligned} \begin{Bmatrix} \varepsilon_x \\ \varepsilon_y \\ \gamma_{xy} \end{Bmatrix} &= \begin{Bmatrix} \varepsilon_x^{(0)} \\ \varepsilon_y^{(0)} \\ \gamma_{xy}^{(0)} \end{Bmatrix} + z \begin{Bmatrix} \varepsilon_x^{(1)} \\ \varepsilon_y^{(1)} \\ \gamma_{xy}^{(1)} \end{Bmatrix} + z^3 \begin{Bmatrix} \varepsilon_x^{(3)} \\ \varepsilon_y^{(3)} \\ \gamma_{xy}^{(3)} \end{Bmatrix} \\ \begin{Bmatrix} \gamma_{yz} \\ \gamma_{xz} \end{Bmatrix} &= \begin{Bmatrix} \gamma_{yz}^{(0)} \\ \gamma_{xz}^{(0)} \end{Bmatrix} + z^2 \begin{Bmatrix} \gamma_{yz}^{(2)} \\ \gamma_{xz}^{(2)} \end{Bmatrix} \end{aligned} \quad (7)$$

Where

$$\varepsilon_x^{(0)} = \frac{\partial u_0}{\partial x} + \frac{1}{2} \left(\frac{\partial w_0}{\partial x} \right)^2, \quad \varepsilon_x^{(1)} = \frac{\partial \varphi_x}{\partial x}, \quad \varepsilon_x^{(3)} = -c_1 \left(\frac{\partial \varphi_x}{\partial x} + \frac{\partial^2 w_0}{\partial x^2} \right)$$

$$\begin{aligned}
\varepsilon_y^{(0)} &= \frac{\partial v_0}{\partial y} + \frac{1}{2} \left(\frac{\partial w_0}{\partial y} \right)^2, \varepsilon_y^{(1)} = \frac{\partial \varphi_y}{\partial y}, \varepsilon_y^{(3)} = -c_1 \left(\frac{\partial \varphi_y}{\partial y} + \frac{\partial^2 w_0}{\partial y^2} \right) \\
\gamma_{xy}^{(0)} &= \frac{\partial u_0}{\partial y} + \frac{\partial v_0}{\partial x} + \frac{\partial w_0}{\partial x} \frac{\partial w_0}{\partial y}, \gamma_{xy}^{(1)} = \frac{\partial \varphi_x}{\partial y} + \frac{\partial \varphi_y}{\partial x}, \gamma_{xy}^{(3)} = -c_1 \left(\frac{\partial \varphi_x}{\partial y} + \frac{\partial \varphi_y}{\partial x} + 2 \frac{\partial^2 w_0}{\partial x \partial y} \right) \\
\gamma_{yz}^{(0)} &= \varphi_y + \frac{\partial w_0}{\partial y}, \gamma_{yz}^{(2)} = -3c_1 \left(\varphi_y + \frac{\partial w_0}{\partial y} \right), \gamma_{xz}^{(0)} = \varphi_x + \frac{\partial w_0}{\partial x}, \\
\gamma_{xz}^{(2)} &= -3c_1 \left(\varphi_x + \frac{\partial w_0}{\partial x} \right)
\end{aligned} \tag{8}$$

2.3 Stresses and force, moment and transverse shear force resultants

The constitutive relationship of Electro-Thermo-Elastic along the material coordinate system is given by Eqs. (9) and (10). Eq. (9) corresponds to the in-plane stress-strain relationship; Eq. (10) corresponds to the shear stress-strain relationship and constitutive relationship for electric displacement due to piezo-electric layers is shown in Eq. (11).

$$\begin{Bmatrix} \sigma_x \\ \sigma_y \\ \sigma_{xy} \end{Bmatrix} = \begin{bmatrix} Q_{11} & Q_{12} & 0 \\ Q_{12} & Q_{22} & 0 \\ 0 & 0 & Q_{66} \end{bmatrix} \left(\begin{Bmatrix} \varepsilon_x \\ \varepsilon_y \\ \gamma_{xy} \end{Bmatrix} - \begin{Bmatrix} \varepsilon_x^T \\ \varepsilon_y^T \\ \gamma_{xy}^T \end{Bmatrix} \right) - \begin{bmatrix} 0 & 0 & e_{31} \\ 0 & 0 & e_{32} \\ e_{15} & 0 & 0 \end{bmatrix} \begin{Bmatrix} E_x \\ E_y \\ E_z \end{Bmatrix} \tag{9}$$

$$\begin{Bmatrix} \sigma_{yz} \\ \sigma_{xz} \end{Bmatrix} = \begin{bmatrix} Q_{44} & 0 \\ 0 & Q_{55} \end{bmatrix} \begin{Bmatrix} \gamma_{yz} \\ \gamma_{xz} \end{Bmatrix} - \begin{bmatrix} 0 & 0 & 0 \\ 0 & e_{24} & 0 \end{bmatrix} \begin{Bmatrix} E_x \\ E_y \\ E_z \end{Bmatrix} \tag{10}$$

$$e_{31} = (d_{31}Q_{11}^a + d_{32}Q_{12}^a), e_{32} = (d_{31}Q_{12}^a + d_{32}Q_{22}^a), e_{24} = d_{24}Q_{44}^a, e_{15} = d_{15}Q_{55}^a \tag{11}$$

Where, $\{\sigma_{ij}\}$ is the stress vector $[Q_{ij}]$ is the constitutive matrix, $\{\varepsilon_{ij}\}$ is the strain vector due to mechanical loading, $\{\varepsilon_{ij}^T\}$ is the strain vector due to thermal loading, $e_{31}, e_{32}, e_{15}, e_{24}$ is the piezoelectric stiffness, $d_{31}, d_{32}, d_{15}, d_{24}$ is the dielectric constants and $Q_{ij}^a (i, j = 1, 2, 4, 5, 6)$ is the elastic stiffness of the piezoelectric actuator layers. The thermal strain vector is given as

$$\begin{Bmatrix} \varepsilon_x^T \\ \varepsilon_y^T \\ \gamma_{xy}^T \end{Bmatrix} = \alpha(z)\Delta T \begin{Bmatrix} 1 \\ 1 \\ 0 \end{Bmatrix} \tag{12}$$

If V_a is the voltage that is applied to the actuators in the thickness direction and E_z as transverse electric field component is dominant in the plate type piezoelectric material, then the electric field vector can be written as

$$\begin{Bmatrix} E_x \\ E_y \\ E_z \end{Bmatrix} = \begin{Bmatrix} 0 \\ 0 \\ 1/h_a \end{Bmatrix} V_a \tag{13}$$

The force, moment and transverse shear force resultants per unit length are related to stress components as

$$\begin{aligned}
\begin{Bmatrix} N_x \\ N_y \\ N_{xy} \end{Bmatrix} &= \int_{-h/2}^{h/2} \begin{Bmatrix} \sigma_x \\ \sigma_y \\ \sigma_{xy} \end{Bmatrix} dz + \int_{-h/2-h_a}^{-h/2} \begin{Bmatrix} \sigma_x^a \\ \sigma_y^a \\ \sigma_{xy}^a \end{Bmatrix} dz + \int_{h/2}^{h/2+h_a} \begin{Bmatrix} \sigma_x^a \\ \sigma_y^a \\ \sigma_{xy}^a \end{Bmatrix} dz \\
\begin{Bmatrix} M_x \\ M_y \\ M_{xy} \end{Bmatrix} &= \int_{-h/2}^{h/2} \begin{Bmatrix} \sigma_x \\ \sigma_y \\ \sigma_{xy} \end{Bmatrix} z dz + \int_{-h/2-h_a}^{-h/2} \begin{Bmatrix} \sigma_x^a \\ \sigma_y^a \\ \sigma_{xy}^a \end{Bmatrix} z dz + \int_{h/2}^{h/2+h_a} \begin{Bmatrix} \sigma_x^a \\ \sigma_y^a \\ \sigma_{xy}^a \end{Bmatrix} z dz \\
\begin{Bmatrix} P_x \\ P_y \\ P_{xy} \end{Bmatrix} &= \int_{-h/2}^{h/2} \begin{Bmatrix} \sigma_x \\ \sigma_y \\ \sigma_{xy} \end{Bmatrix} z^3 dz + \int_{-h/2-h_a}^{-h/2} \begin{Bmatrix} \sigma_x^a \\ \sigma_y^a \\ \sigma_{xy}^a \end{Bmatrix} z^3 dz + \int_{h/2}^{h/2+h_a} \begin{Bmatrix} \sigma_x^a \\ \sigma_y^a \\ \sigma_{xy}^a \end{Bmatrix} z^3 dz \\
\begin{Bmatrix} R_x \\ R_y \end{Bmatrix} &= \int_{-h/2}^{h/2} \begin{Bmatrix} \sigma_{xz} \\ \sigma_{yz} \end{Bmatrix} z^2 dz + \int_{-h/2-h_a}^{-h/2} \begin{Bmatrix} \sigma_{xz}^a \\ \sigma_{yz}^a \end{Bmatrix} z^2 dz + \int_{h/2}^{h/2+h_a} \begin{Bmatrix} \sigma_{xz}^a \\ \sigma_{yz}^a \end{Bmatrix} z^2 dz \\
\begin{Bmatrix} Q_x \\ Q_y \end{Bmatrix} &= \int_{-h/2}^{h/2} \begin{Bmatrix} \sigma_{xz} \\ \sigma_{yz} \end{Bmatrix} dz + \int_{-h/2-h_a}^{-h/2} \begin{Bmatrix} \sigma_{xz}^a \\ \sigma_{yz}^a \end{Bmatrix} dz + \int_{h/2}^{h/2+h_a} \begin{Bmatrix} \sigma_{xz}^a \\ \sigma_{yz}^a \end{Bmatrix} dz
\end{aligned} \tag{14}$$

Substituting Eqs. (9)-(11) and (7) into Eqs. (14) gives

$$\begin{aligned}
\begin{Bmatrix} \{N\} \\ \{M\} \\ \{P\} \end{Bmatrix} &= \begin{bmatrix} [A_{ij}] & [B_{ij}] & [E_{ij}] \\ [B_{ij}] & [D_{ij}] & [F_{ij}] \\ [E_{ij}] & [F_{ij}] & [H_{ij}] \end{bmatrix} \begin{Bmatrix} \{\varepsilon^{(0)}\} \\ \{\varepsilon^{(1)}\} \\ \{\varepsilon^{(3)}\} \end{Bmatrix} - \begin{Bmatrix} \{N^T\} \\ \{M^T\} \\ \{P^T\} \end{Bmatrix} \\
\begin{Bmatrix} \{Q\} \\ \{R\} \end{Bmatrix} &= \begin{bmatrix} [A_{ij}] & [D_{ij}] \\ [D_{ij}] & [F_{ij}] \end{bmatrix} \begin{Bmatrix} \{\gamma^{(0)}\} \\ \{\gamma^{(2)}\} \end{Bmatrix}
\end{aligned} \tag{15}$$

where the subscripts 'T' and 'a' signal the thermal and electric loads, respectively. Here $[A_{ij}]$ denote the stretching stiffness matrix, $[D_{ij}]$ the bending stiffness matrix, $[B_{ij}]$ the stretching-bending coupling stiffness matrix, and $([E_{ij}], [F_{ij}], [H_{ij}])$ are the higher-order stiffness matrix.

$$([A_{ij}], [B_{ij}], [D_{ij}], [E_{ij}], [F_{ij}], [H_{ij}]) = \int_{-h/2}^{h/2} [Q_{ij}](1, z, z^2, z^3, z^4, z^6) dz \tag{16}$$

Thermal force and piezoelectric resultants are calculated as

$$\begin{Bmatrix} N_x^T & M_x^T \\ N_y^T & M_y^T \\ N_{xy}^T & M_{xy}^T \end{Bmatrix} = \int_{-h/2}^{h/2} \begin{bmatrix} Q_{11} & Q_{12} & 0 \\ Q_{12} & Q_{22} & 0 \\ 0 & 0 & Q_{66} \end{bmatrix} \begin{Bmatrix} \alpha(z) \\ \alpha(z) \\ 0 \end{Bmatrix} (1, z) \Delta T dz +$$

$$\begin{aligned}
& + \int_{-\frac{h}{2}-h_a}^{-\frac{h}{2}} \begin{bmatrix} Q_{11}^a & Q_{12}^a & 0 \\ Q_{12}^a & Q_{21}^a & 0 \\ 0 & 0 & Q_{66}^a \end{bmatrix} \begin{Bmatrix} \alpha_{11}^a \\ \alpha_{22}^a \\ 0 \end{Bmatrix} (1, z) \Delta T dz \\
& + \int_{h/2}^{h/2+h_a} \begin{bmatrix} Q_{11}^a & Q_{12}^a & 0 \\ Q_{12}^a & Q_{21}^a & 0 \\ 0 & 0 & Q_{66}^a \end{bmatrix} \begin{Bmatrix} \alpha_{11}^a \\ \alpha_{22}^a \\ 0 \end{Bmatrix} (1, z) \Delta T dz
\end{aligned} \tag{17a}$$

and

$$\begin{Bmatrix} N_x^a & M_x^a \\ N_y^a & M_y^a \\ N_{xy}^a & M_{xy}^a \end{Bmatrix} = \int_{-h/2-h_a}^{-h/2} \begin{Bmatrix} e_{31} \\ e_{32} \\ 0 \end{Bmatrix} (1, z) \frac{V}{h_a} dz + \int_{h/2}^{h/2+h_a} \begin{Bmatrix} e_{31} \\ e_{32} \\ 0 \end{Bmatrix} (1, z) \frac{V}{h_a} dz \tag{17b}$$

2.4 Equations of stability

The stability equations of a piezoelectric FGM rectangular plate by TSDT are

$$\begin{aligned}
\frac{\partial N_x}{\partial x} + \frac{\partial N_{xy}}{\partial y} &= 0 \\
\frac{\partial N_{xy}}{\partial x} + \frac{\partial N_y}{\partial y} &= 0 \\
\frac{\partial Q_x}{\partial x} + \frac{\partial Q_y}{\partial y} - 3c_1 \left(\frac{\partial R_x}{\partial x} + \frac{\partial R_y}{\partial y} \right) + c_1 \left(\frac{\partial^2 P_x}{\partial x^2} + 2 \frac{\partial^2 P_{xy}}{\partial x \partial y} + \frac{\partial^2 P_y}{\partial y^2} \right) + \bar{N} &= 0 \\
\frac{\partial M_x}{\partial x} + \frac{\partial M_{xy}}{\partial y} - Q_x + 3c_1 R_x - c_1 \left(\frac{\partial P_x}{\partial x} + \frac{\partial P_{xy}}{\partial y} \right) &= 0 \\
\frac{\partial M_{xy}}{\partial x} + \frac{\partial M_y}{\partial y} - Q_y + 3c_1 R_y - c_1 \left(\frac{\partial P_{xy}}{\partial x} + \frac{\partial P_y}{\partial y} \right) &= 0
\end{aligned} \tag{18}$$

With

$$\bar{N} = (N_x^m + N_x^a) \frac{\partial^2 w}{\partial x^2} + (N_y^m + N_y^a) \frac{\partial^2 w}{\partial y^2} + 2(N_{xy}^m + N_{xy}^a) \frac{\partial^2 w}{\partial x \partial y} \tag{19}$$

Where N_x^m, N_y^m, N_{xy}^m and N_x^a, N_y^a, N_{xy}^a are, respectively, the mechanical and constant applied actuator voltage forces with

$$\begin{aligned}
N_x^m &= N_y^m = - \frac{\int_{-h/2}^{h/2} E(z) \alpha(z) \Delta T dz}{1-\nu}; \\
N_{xy}^m &= 0 \\
N_x^a &= N_y^a = -2V_a (d_{31} Q_{11}^a + d_{32} Q_{12}^a); \\
N_y^a &= -2V_a (d_{31} Q_{12}^a + d_{32} Q_{22}^a); \\
N_{xy}^a &= 0
\end{aligned} \tag{20}$$

According to Eqs. (18a), (18e) and equilibrium equations, the governing equations including

the effects of thermal environment and piezoelectric layers are expressed as

$$A_{11} \frac{\partial^2 u_0}{\partial x^2} + A_{12} \frac{\partial^2 v_0}{\partial x \partial y} + B_{11} \frac{\partial^2 \varphi_x}{\partial x^2} + B_{12} \frac{\partial^2 \varphi_y}{\partial x \partial y} - c_1 E_{11} \left(\frac{\partial^2 \varphi_x}{\partial x^2} + \frac{\partial^3 w_0}{\partial x^3} \right) - c_1 E_{12} \left(\frac{\partial^2 \varphi_y}{\partial x \partial y} + \frac{\partial^3 w_0}{\partial x \partial y^2} \right) + A_{66} \left(\frac{\partial^2 u_0}{\partial y^2} + \frac{\partial^2 v_0}{\partial x \partial y} \right) + B_{66} \left(\frac{\partial^2 \varphi_x}{\partial y^2} + \frac{\partial^2 \varphi_y}{\partial x \partial y} \right) - c_1 E_{66} \left(\frac{\partial^2 \varphi_x}{\partial y^2} + \frac{\partial^2 \varphi_y}{\partial x \partial y} + 2 \frac{\partial^3 w_0}{\partial x \partial y^2} \right) - \frac{\partial N_x^T}{\partial x} - \frac{\partial Z_1^a}{\partial x} = 0 \quad (21a)$$

$$A_{66} \left(\frac{\partial^2 u_0}{\partial x \partial y} + \frac{\partial^2 v_0}{\partial x^2} \right) + B_{66} \left(\frac{\partial^2 \varphi_x}{\partial x \partial y} + \frac{\partial^2 \varphi_y}{\partial x^2} \right) - c_1 E_{66} \left(\frac{\partial^2 \varphi_x}{\partial x \partial y} + \frac{\partial^2 \varphi_y}{\partial x^2} + 2 \frac{\partial^3 w_0}{\partial x^2 \partial y} \right) + A_{12} \frac{\partial^2 u_0}{\partial x \partial y} + A_{22} \frac{\partial^2 v_0}{\partial y^2} + B_{12} \frac{\partial^2 \varphi_x}{\partial x \partial y} + B_{22} \frac{\partial^2 \varphi_y}{\partial y^2} - c_1 E_{12} \left(\frac{\partial^2 \varphi_x}{\partial x \partial y} + \frac{\partial^3 w_0}{\partial x^2 \partial y} \right) - c_1 E_{22} \left(\frac{\partial^2 \varphi_y}{\partial y^2} + \frac{\partial^3 w_0}{\partial y^3} \right) - \frac{\partial N_y^T}{\partial x} - \frac{\partial Z_4^a}{\partial x} = 0 \quad (21b)$$

$$A_{55} \left(\frac{\partial \varphi_x}{\partial x} + \frac{\partial^2 w_0}{\partial x^2} \right) - 6c_1 D_{55} \left(\frac{\partial \varphi_x}{\partial x} + \frac{\partial^2 w_0}{\partial x^2} \right) + 9c_1^2 F_{55} \left(\frac{\partial \varphi_x}{\partial x} + \frac{\partial^2 w_0}{\partial x^2} \right) + A_{44} \left(\frac{\partial^2 \varphi_y}{\partial y} + \frac{\partial^2 w_0}{\partial y^2} \right) + c_1 \left[E_{11} \frac{\partial^3 u_0}{\partial x^3} + E_{12} \left(\frac{\partial^3 u_0}{\partial x \partial y^2} + \frac{\partial^3 v_0}{\partial x^2 \partial y} \right) + E_{22} \frac{\partial^3 v_0}{\partial y^3} + F_{11} \frac{\partial^3 \varphi_x}{\partial x^3} + F_{12} \left(\frac{\partial^3 \varphi_x}{\partial x \partial y^2} + \frac{\partial^3 \varphi_y}{\partial x^2 \partial y} \right) + F_{22} \frac{\partial^3 \varphi_y}{\partial y^3} \right] - c_1^2 \left[H_{11} \left(\frac{\partial^3 \varphi_x}{\partial x^3} + \frac{\partial^4 w_0}{\partial x^4} \right) + H_{12} \left(\frac{\partial^3 \varphi_x}{\partial x \partial y^2} + \frac{\partial^3 \varphi_y}{\partial x^2 \partial y} + 2 \frac{\partial^4 w_0}{\partial x^2 \partial y^2} \right) + H_{22} \left(\frac{\partial^3 \varphi_y}{\partial y^3} + \frac{\partial^4 w_0}{\partial y^4} \right) \right] - 2c_1^2 H_{66} \left(\frac{\partial^3 \varphi_x}{\partial x \partial y^2} + \frac{\partial^3 \varphi_y}{\partial x^2 \partial y} + 2 \frac{\partial^4 w_0}{\partial x^2 \partial y^2} \right) + c_1 \left[2E_{66} \left(\frac{\partial^3 u}{\partial x \partial y^2} + \frac{\partial^3 v}{\partial x^2 \partial y} \right) + 2F_{66} \left(\frac{\partial^3 \varphi_x}{\partial x \partial y^2} + \frac{\partial^3 \varphi_y}{\partial x^2 \partial y} \right) \right] \quad (21c)$$

$$-A_{55} \left(\varphi_x + \frac{\partial w_0}{\partial x} \right) + 6c_1 D_{55} \left(\varphi_x + \frac{\partial w_0}{\partial x} \right) - 9c_1^2 F_{55} \left(\varphi_x + \frac{\partial w_0}{\partial x} \right) + B_{11} \frac{\partial^2 u_0}{\partial x^2} + B_{12} \frac{\partial^2 v_0}{\partial x \partial y} + D_{11} \frac{\partial^2 \varphi_x}{\partial x^2} + D_{12} \frac{\partial^2 \varphi_y}{\partial x \partial y} - c_1 F_{11} \left(2 \frac{\partial^2 \varphi_x}{\partial x^2} + \frac{\partial^3 w_0}{\partial x^3} \right) - c_1 F_{12} \left(2 \frac{\partial^2 \varphi_y}{\partial x \partial y} + \frac{\partial^3 w_0}{\partial x \partial y^2} \right) - c_1 \left[E_{11} \frac{\partial^2 u_0}{\partial x^2} + E_{12} \frac{\partial^2 v_0}{\partial x \partial y} \right] + c_1^2 \left[H_{11} \left(\frac{\partial^2 \varphi_x}{\partial x^2} + \frac{\partial^3 w_0}{\partial x^3} \right) + H_{12} \left(\frac{\partial^2 \varphi_y}{\partial x \partial y} + \frac{\partial^3 w_0}{\partial x \partial y^2} \right) \right] + B_{66} \left(\frac{\partial^2 u_0}{\partial y^2} + \frac{\partial^2 v_0}{\partial x \partial y} \right) + D_{66} \left(\frac{\partial^2 \varphi_x}{\partial y^2} + \frac{\partial^2 \varphi_y}{\partial x \partial y} \right) - 2c_1 F_{66} \left(\frac{\partial^2 \varphi_x}{\partial y^2} + \frac{\partial^2 \varphi_y}{\partial x \partial y} + \frac{\partial^3 w_0}{\partial x \partial y^2} \right) - c_1 E_{66} \left(\frac{\partial^2 u_0}{\partial y^2} + \frac{\partial v_0}{\partial x \partial y} \right) + c_1^2 H_{66} \left(\frac{\partial^2 \varphi_x}{\partial y^2} + \frac{\partial^2 \varphi_y}{\partial x \partial y} + 2 \frac{\partial^3 w_0}{\partial x \partial y^2} \right) - \frac{\partial M_x^T}{\partial x} - \frac{\partial Z_2^a}{\partial x} + c_1 \frac{\partial P_x^T}{\partial x} - \frac{\partial Z_3^a}{\partial x} = 0 \quad (21d)$$

$$-A_{44} \left(\varphi_y + \frac{\partial w_0}{\partial y} \right) + 6c_1 D_{44} \left(\varphi_y + \frac{\partial w_0}{\partial y} \right) - 9c_1^2 F_{44} \left(\varphi_y + \frac{\partial w_0}{\partial y} \right) + B_{12} \frac{\partial^2 u_0}{\partial x \partial y} + B_{22} \frac{\partial^2 v_0}{\partial y^2} + D_{12} \frac{\partial^2 \varphi_x}{\partial x \partial y} + D_{22} \frac{\partial^2 \varphi_y}{\partial y^2} - c_1 \left[F_{12} \left(2 \frac{\partial^2 \varphi_x}{\partial x \partial y} + \frac{\partial^3 w_0}{\partial x \partial y^2} \right) + F_{22} \left(2 \frac{\partial^2 \varphi_y}{\partial y^2} + \frac{\partial^3 w_0}{\partial y^3} \right) + 2F_{66} \left(\frac{\partial^2 \varphi_x}{\partial x \partial y} + \frac{\partial^2 \varphi_y}{\partial x^2} + \frac{\partial^3 w_0}{\partial x \partial y^2} \right) \right] - c_1 \left[E_{12} \frac{\partial^2 u_0}{\partial x \partial y} + E_{22} \frac{\partial^2 v_0}{\partial y^2} + E_{66} \left(\frac{\partial^2 u_0}{\partial x \partial y} + \frac{\partial v_0}{\partial x^2} \right) \right] + c_1^2 \left[H_{12} \left(\frac{\partial^2 \varphi_x}{\partial x \partial y} + \frac{\partial^3 w_0}{\partial x^2 \partial y} \right) + H_{22} \left(\frac{\partial^2 \varphi_y}{\partial y^2} + \frac{\partial^3 w_0}{\partial y^3} \right) \right] + B_{66} \left(\frac{\partial^2 u_0}{\partial x \partial y} + \frac{\partial^2 v_0}{\partial x^2} \right) + D_{66} \left(\frac{\partial^2 \varphi_x}{\partial x \partial y} + \frac{\partial^2 \varphi_y}{\partial x^2} \right) + c_1^2 H_{66} \left(\frac{\partial^2 \varphi_x}{\partial x \partial y} + \frac{\partial^2 \varphi_y}{\partial x^2} + 2 \frac{\partial^3 w_0}{\partial x^2 \partial y} \right) - \frac{\partial M_y^T}{\partial y} - \frac{\partial Z_5^a}{\partial y} + c_1 \frac{\partial P_y^T}{\partial y} - \frac{\partial Z_6^a}{\partial y} = 0 \quad (21e)$$

The following approximate solution is seen to satisfy both the differential equation and the boundary conditions

$$\begin{Bmatrix} u_0 \\ v_0 \\ w_0 \\ \varphi_x \\ \varphi_y \end{Bmatrix} = \sum_{m=1}^{\infty} \sum_{n=1}^{\infty} \begin{Bmatrix} U_{mn} \cos \lambda x \sin \mu y \\ V_{mn} \sin \lambda x \cos \mu y \\ W_{mn} \sin \lambda x \sin \mu y \\ X_{mn} \cos \lambda x \sin \mu y \\ Y_{mn} \sin \lambda x \cos \mu y \end{Bmatrix} \quad (22)$$

Substitution of Eq. (22) into Eqs. (21a)-(21e), we obtain a 5×5 system of the differential equations

$$\begin{bmatrix} S_{11} & S_{12} & S_{13} & S_{14} & S_{15} \\ S_{12} & S_{22} & S_{23} & S_{24} & S_{25} \\ S_{13} & S_{23} & S_{33} & S_{34} & S_{35} \\ S_{14} & S_{24} & S_{34} & S_{44} & S_{45} \\ S_{15} & S_{25} & S_{35} & S_{45} & S_{55} \end{bmatrix} \begin{pmatrix} U_{mn} \\ V_{mn} \\ W_{mn} \\ X_{mn} \\ Y_{mn} \end{pmatrix} = \begin{pmatrix} 0 \\ 0 \\ 0 \\ 0 \\ 0 \end{pmatrix} \quad (23)$$

where S_{ij} is defined by

$$\begin{aligned} s_{11} &= A_{11}\lambda^2 + A_{66}\mu^2, s_{12} = \lambda\mu(A_{12} + A_{66}), \\ s_{13} &= -c_1 \lambda[E_{11}\lambda^2 + (E_{12} + 2E_{66})\mu^2], \\ s_{14} &= (B_{11} - c_1 E_{11})\lambda^2 + (B_{66} - c_1 E_{66})\mu^2, \\ s_{15} &= [(B_{12} - c_1 E_{12}) + (B_{66} - c_1 E_{66})]\lambda\mu, \\ s_{22} &= A_{66}\lambda^2 + A_{22}\mu^2, \\ s_{23} &= -c_1 \mu[(E_{12} + 2E_{66})\lambda^2 + E_{22}\mu^2], \\ s_{24} &= s_{15}, \\ s_{25} &= (B_{66} - c_1 E_{66})\lambda^2 + (B_{22} - c_1 E_{22})\mu^2 \\ s_{33} &= (A_{55} - 6c_1 D_{55})\lambda^2 + (A_{44} - 6c_1 D_{44})\mu^2 + N_x^0\lambda^2 + N_y^0\mu^2 \\ &+ c_1^2[H_{11}\lambda^4 + 2(H_{12} + 2H_{66})\lambda^2\mu^2 + H_{22}\mu^4 + 9F_{44}\mu^2 + 9F_{55}\lambda^2] \\ s_{34} &= (A_{55} - 6c_1 D_{55} + 9c_1^2 F_{55})\lambda \\ &- c_1 [(F_{11} - c_1 H_{11})\lambda^3 + ((F_{12} - c_1 H_{12}) + 2(F_{66} - c_1 H_{66}))\lambda\mu^2] \\ s_{35} &= (A_{44} - 6c_1 D_{44} + 9c_1^2 F_{44})\mu \\ &- c_1 [(F_{22} - c_1 H_{22})\mu^3 + ((F_{12} - c_1 H_{12}) + 2(F_{66} - c_1 H_{66}))\lambda^2\mu] \\ s_{44} &= A_{55} - 6c_1 D_{55} + 9c_1^2 F_{55} + (D_{11} - 2c_1 F_{11} + c_1^2 H_{11})\lambda^2 \\ &+ (D_{66} - 2c_1 F_{66} + c_1^2 H_{66})\mu^2 \\ s_{45} &= [(D_{12} - 2c_1 F_{12} + c_1^2 H_{12}) + (D_{66} - 2c_1 F_{66} + c_1^2 H_{66})]\lambda\mu \\ s_{55} &= A_{44} - 6c_1 D_{44} + 9c_1^2 F_{44} + (D_{66} - 2c_1 F_{66} + c_1^2 H_{66})\lambda^2 \\ &+ (D_{22} - 2c_1 F_{22} + c_1^2 H_{22})\mu^2 \end{aligned} \quad (24)$$

2.5 Uniform temperature loads rise

The plate initial temperature is assumed to be T_i . The temperature is uniformly raised to a final value T_f in which the piezoelectric porous FGM plate buckles. The temperature change is given by (Bouazza *et al.* 2016, 2019, 2021)

$$\Delta T = T_f - T_i \quad (25)$$

Table 1 Material properties of FGMs and piezoelectric materials

Properties	Aluminum	Alumina	G-1195N
E (GPa)	70	380	63.0
ν	0.3	0.3	0.3
α (1/°C)	23×10^{-6}	10.4×10^{-6}	1.2×10^{-6}
k (W/mK)	2.09	204	5.0
d_{31} (m/V)	--	--	2.54×10^{-10}
d_{31} (m/V)	--	--	2.54×10^{-10}

Table 2 Comparison of critical buckling temperature of simply supported isotropic plates ($a/h = 100$, $\nu = 0.3$, $\alpha = 1.0 \times 10^{-6}$)

a/b	Chen (1991)	Ganapathi (1997)	Chun-Sheng (2011)	Present Results
0.25	0.691	0.676	0.672	0.6720
0.50	0.814	0.789	0.791	0.7905
1.0	1.319	1.272	1.264	1.2646
1.50	2.101	2.072	2.054	2.0543
2.0	3.191	3.176	3.158	3.1589
2.5	4.601	4.585	4.578	4.5775
3.0	6.330	6.341	6.306	6.3089

Table 3 Comparison of critical buckling of simply supported square isotropic plate under

a/h	Matsunaga (2005)	Bourada <i>et al.</i> (2012)	Kettaf <i>et al.</i> (2013)	Fethi (2019)	Present
10	$0,1183 \times 10^{-1}$	$0,1198 \times 10^{-1}$	$0,1198 \times 10^{-1}$	$0,1198 \times 10^{-1}$	$0,1198 \times 10^{-1}$
20	$0,3109 \times 10^{-2}$	$0,3119 \times 10^{-2}$	$0,3119 \times 10^{-2}$	$0,3119 \times 10^{-2}$	$0,3119 \times 10^{-2}$
100	$0,1264 \times 10^{-3}$	$0,1265 \times 10^{-3}$	$0,1265 \times 10^{-3}$	$0,1265 \times 10^{-3}$	$0,1265 \times 10^{-3}$

3. Numerical results and discussion

3.1 Validation of results

FGM with a mixture of aluminum and alumina for the FGM substrate and G-1195N for the piezoelectric layers is used for the plate, which is referred to as Al/Al₂O₃. The actuator layer thickness is $ha=0.001$ m. The material properties for aluminum, alumina, and G-1195N are listed in Table 1.

The comparison is performed for simply supported isotropic plates subjected to under uniform temperature rise for different values of aspect ratio (a/b) are shown in Table 2. The thickness ratio of the plate is set as ($a/h=100$). The critical temperature buckling loads of present theory are compared with the results of Chen *et al.* (1991), Ganapathi (1997), Chun-Sheng (2011) results. They are in excellent agreement.

Table 3 presents the critical temperature comparison $\alpha \Delta T_{cr}$ of a simply supported square isotropic plate under uniform temperature with ($E = 10^{-6}$ N/m² and $\alpha = 10^{-6}$ 1/K). The results obtained from the present theory are compared to those obtained by Matsunaga (2005), Bourada *et al.* (2012), Kettaf *et al.* (2013). According to this table, this can be seen as excellent agreement with these current results and those given in the literature.

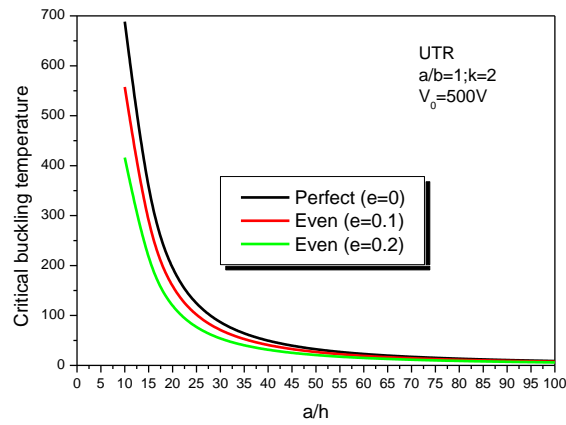


Fig. 5 Critical buckling temperature of piezoelectric porous FGM-I plate under uniform temperature rise vs of side-to-thickness ratio of the plate (a/h)

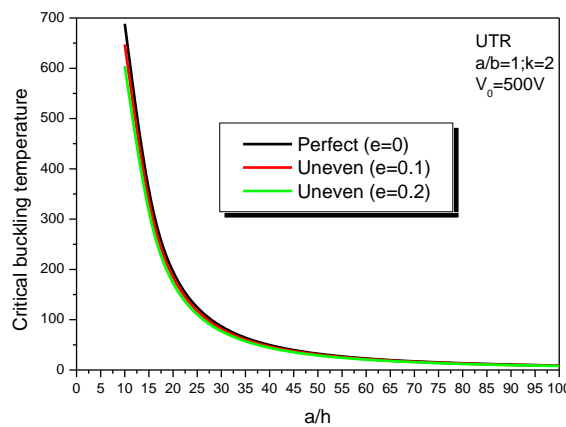


Fig. 6 Critical buckling temperature of piezoelectric porous FGM-II plate under uniform temperature rise vs of side-to-thickness ratio of the plate (a/h)

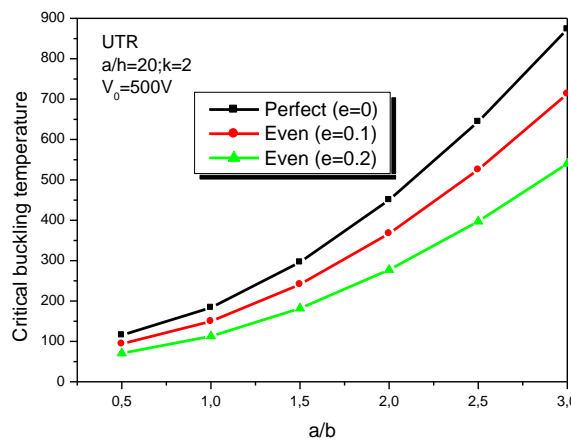


Fig. 7 Critical buckling temperature of piezoelectric porous FGM-I plate under uniform temperature rise vs aspect ratio of the plate (a/b)

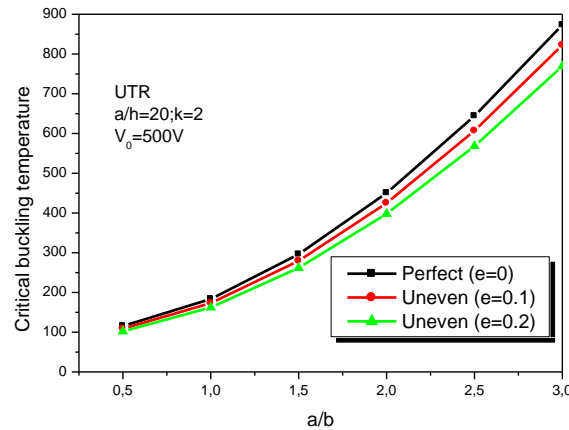


Fig. 8 Critical buckling temperature of piezoelectric porous FGM-I plate under uniform temperature rise vs aspect ratio of the plate (a/b)

3.2 Parametric studies

Firstly, the influence of side-to-thickness ratio (a/h) on the thermal buckling load with various values of porosity coefficient (e) for a simply supported square with even and uneven porosity distributions is plotted in Figs. 5 and 6, respectively, at the volume fractions of the constituents ($k=2$), when the applying voltage is ($V_0=500$) and porosity parameters ($e=0, 0.1, 0.2$). It is clear that a perfect piezoelectric FGM plate has higher buckling loads than porous FGM piezoelectric plate at a constant electric voltage. Also, it is observable from these Fig. 5 that the effect of porosity coefficient is significant when the side-to-thickness ratio value is smaller, but it is ignorable at large side-to-thickness ratios.

Figs. 7 and 8 depict the effect of plate aspect ratio (a/b) on critical buckling temperature for two types of porosity distribution called even and uneven, respectively and simply boundary conditions. The piezoelectric FGM plate is made of porous functionally graded materials that are integrated with surface bonded piezoelectric Layers. The side-to-thickness ratio of the PFGM plate is set as $a/h=20$, volume fractions of the constituents ($k=2$), the applying voltage is ($V_0=500$) and different values of porosity parameters ($e=0, 0.1, 0.2$). It is observed that with increasing the plate aspect ratio a/b from 0.5 to 3, the critical buckling temperature difference also increases steadily, whatever the porosity parameters (e) is.

4. Conclusions

The thermal buckling of FG porous layer with integrated with surface-bonded piezoelectric actuator layers with simply boundary conditions and two different porosity distributions have been investigated. Two kinds of porosity distribution called even and uneven were considered. A modified power-law function was employed to describe the graded and porosity-dependent material properties. Theoretical formulations are within the framework of third-order shear deformation plate theory. Navier method is employed to obtain the thermal critical buckling load. The effects of porosity coefficient (e) and thickness ratio (a/h), and aspect ratio (a/b) on the

thermal critical buckling load are discussed. Numerical results show that:

- An increase in the porosity coefficient and side-to-thickness ratio leads to lower thermal critical buckling loads of piezoelectric functionally graded porous plates.
- The critical buckling temperature can be controlled by applying a suitable voltage on the actuator layers
- The critical buckling temperature will increase by increasing the thickness.
- The porosity distribution has a significant influence on the critical buckling temperature behavior of the plate.
- The critical buckling temperature of the piezoelectric FGM plate is more sensitive when the pores are evenly distributed.
- The plates with uneven distribution usually provide higher critical buckling temperature compared with that of FGM-I plates. The trend for variation of critical buckling temperature with respect to porosity parameter is dependent upon the value of power law index (k).

References

- Amara, K., Bouazza, M. and Fouad, B. (2016), "Postbuckling analysis of functionally graded beams using nonlinear model", *Periodica Polytechnica Mech. Eng.*, **60**(2), 121-128. <https://doi.org/10.3311/PPme.8854>.
- Arefi, M. and Rahimi, G.H. (2012), "Studying the nonlinear behavior of the functionally graded annular plates with piezoelectric layers as a sensor and actuator under normal pressure", *Smart Struct. Syst.*, **9**(2), 127-143. <https://doi.org/10.12989/sss.2012.9.2.127>.
- Avsar, A.L. and Sahin, M. (2016), "Bimorph piezoelectric energy harvester structurally integrated on a trapezoidal plate", *Smart Struct. Syst.*, **18**(2), 249-265. <https://doi.org/10.12989/sss.2016.18.2.249>.
- Becheri, T., Amara, K., Bouazza, M. and Benseddiq, N. (2016), "Buckling of symmetrically laminated plates using nth-order shear deformation theory with curvature effects", *Steel Compos. Struct.*, **21**(6), 1347-1368. <https://doi.org/10.12989/scs.2016.21.6.1347>.
- Boley, B.A. and Weiner, J.J (1960), *Theory of Thermal Stresses*, John Wiley, New York.
- Bouazza, M. and Adda-Bedia, E.A. (2013), "Elastic stability of functionally graded rectangular plates under mechanical and thermal loadings", *Acad. J., Scientif. Res. Essay.*, **8**(39), 1933-1943. <https://doi.org/10.5897/SRE11.251>.
- Bouazza, M. and Zenkour, A.M. (2021), "Hygrothermal environmental effect on free vibration of laminated plates using nth-order shear deformation theory", *Wave. Random Complex Media*, 1-17. <https://doi.org/10.1080/17455030.2021.1909173>.
- Bouazza, M., Amara, K. and Benseddiq, N. (2017), "Mechanical buckling analysis of functionally graded plates using a new refined theory", *Jordan J. Civil Eng.*, **11**(1), 64.
- Bouazza, M., Antar, K., Amara, K., Benyoucef, S. and Bedia, E. (2019), "Influence of temperature on the beams behavior strengthened by bonded composite plates", *Geomech. Eng.*, **18**(5), 555-566. <https://doi.org/10.12989/gae.2019.18.5.555>.
- Bouazza, M., Becheri, T., Boucheta, A. and Benseddiq, N. (2019), "Bending behavior of laminated composite plates using the refined four-variable theory and the finite element method", *Earthq. Struct.*, **17**(3), 257-270. <https://doi.org/10.12989/eas.2019.17.3.257>.
- Bouazza, M., Becheri, T., Boucheta, A. and Benseddiq, N. (2016), "Thermal buckling analysis of nanoplates based on nonlocal elasticity theory with four-unknown shear deformation theory resting on Winkler-Pasternak elastic foundation", *Int. J. Comput. Meth. Eng. Sci. Mech.*, **17**(5-6), 362-373. <https://doi.org/10.1080/15502287.2016.1231239>.
- Bouazza, M., Benseddiq, N. and Zenkour, A.M. (2019), "Thermal buckling analysis of laminated composite beams using hyperbolic refined shear deformation theory", *J. Therm. Stress.*, **42**(3), 332-340.

- <https://doi.org/10.1080/01495739.2018.1461042>.
- Bouazza, M., Boucheta, A., Becheri, T. and Benseddiq, N. (2017), "Thermal stability analysis of functionally graded plates using simple refined plate theory", *Int. J. Autom. Mech. Eng.*, **14**(1), 4013-4029. <https://doi.org/10.15282/ijame.14.1.2017.15.0325>.
- Bourada, M., Tounsi, A., Houari, M.S.A. and Bedia, E.A.A. (2012), "A new four-variable refined plate theory for thermal buckling analysis of functionally graded sandwich plates", *J. Sandw. Struct. Mater.*, **14**(1), 5-33. <https://doi.org/10.1177/1099636211426386>.
- Chaudhary, S.K., Kar, V.R. and Shukla, K.K. (2023), "Thermoelastic deformation behavior of functionally graded cylindrical panels with multiple perforations", *Adv. Aircraft Spacecraft Sci.*, **10**(2), 127-140. <https://doi.org/10.12989/aas.2023.10.2.127>.
- Chen, W.J., Lin, P.D. and Chen, L.W. (1991), "Thermal buckling behavior of thick composite laminated plates under nonuniform temperature distribution", *Comput. Struct.*, **41**(4), 637-645. [https://doi.org/10.1016/0045-7949\(91\)90176-M](https://doi.org/10.1016/0045-7949(91)90176-M).
- Ebrahimi, F. and Barati, M. (2018), "Surface and flexoelectricity effects on size-dependent thermal stability analysis of smart piezoelectric nanoplates", *Struct. Eng. Mech.*, **67**(2), 143-153. <https://doi.org/10.12989/sem.2018.67.2.143>.
- Ebrahimi, F., Seyfi, A., Dabbag, H.A. and Tornabene, F. (2019), "Wave dispersion characteristics of porous graphene platelet reinforced composite shells", *Struct. Eng. Mech.*, **71**(1), 99-107. <https://doi.org/10.12989/sem.2019.71.1.099>.
- Ellali, M., Amara, K., Bouazza, M. and Bourada, F. (2018), "The buckling of piezoelectric plates on pasternak elastic foundation using higher-order shear deformation plate theories", *Smart Struct. Syst.*, **21**(1), 113-122. <https://doi.org/10.12989/sss.2018.21.1.113>.
- Ellali, M., Bouazza, M. and Zenkour, A.M. (2024), "Hygrothermal vibration of FG nanobeam via nonlocal unknown integral variables secant-tangential shear deformation coupled theory with temperature-dependent material properties", *Eur. J. Mech.-A/Solid.*, **105**, 105243. <https://doi.org/10.1016/j.euromechsol.2024.105243>.
- Ellali, M., Bouazza, M. and Zenkour, A.M. (2022), "Impact of micromechanical approaches on wave propagation of FG plates via indeterminate integral variables with a hyperbolic secant shear model", *Int. J. Comput. Meth.*, **19**(9), 2250019. <https://doi.org/10.1142/S0219876222500190>.
- Ellali, M., Bouazza, M. and Zenkour, A.M. (2023), "Wave propagation of FGM plate via new integral inverse cotangential shear model with temperature-dependent material properties", *Geomech. Eng.*, **33**(5), 427-437. <https://doi.org/10.12989/gae.2023.33.5.427>.
- Fenjan, R.M., Ahmed, R.A., Alasadi, A.A. and Faleh, N.M. (2019), "Nonlocal strain gradient thermal vibration analysis of double-coupled metal foam plate system with uniform and non-uniform porosities", *Couple. Syst. Mech.*, **8**(3), 247-257. <https://doi.org/10.12989/csm.2019.8.3.247>.
- Ganapathi, M. and Touratier, M. (1997), "A study on thermal postbuckling behaviour of laminated composite plates using a shear-flexible finite element", *Finite Elem. Anal. Des.*, **28**(2), 115-135. [https://doi.org/10.1016/S0168-874X\(97\)81955-5](https://doi.org/10.1016/S0168-874X(97)81955-5).
- Ghasemabadian, M.A. and Kadkhodayan, M. (2016), "Investigation of buckling behavior of functionally graded piezoelectric (FGP) rectangular plates under open and closed circuit conditions", *Struct. Eng. Mech.*, **60**(2), 271-299. <https://doi.org/10.12989/sem.2016.60.2.271>.
- Ghasemabadian, M.A. and Saidi, A.R. (2017), "Stability analysis of transversely isotropic laminated Mindlin plates with piezoelectric layers using a Levy-type solution", *Struct. Eng. Mech.*, **62**(6), 675-693. <https://doi.org/10.12989/sem.2017.62.6.675>.
- Guessas, H., Zidour, M., Meradjah, M. and Tounsi, A. (2018), "The critical buckling load of reinforced nanocomposite porous plates", *Struct. Eng. Mech.*, **67**(2), 115-123. <https://doi.org/10.12989/sem.2018.67.2.115>.
- Hussain, M.A. (2014), "Buckling analysis of functionally graded carbon nanotubes reinforced composite (FG-CNTRC) plate", Doctoral Dissertation, National Institute of Technology Rourkela, Odisha, India.
- Kar, V.R. and Panda, S.K. (2017), "Postbuckling analysis of shear deformable FG shallow spherical shell panel under nonuniform thermal environment", *J. Therm. Stress.*, **40**(1), 25-39.

- <https://doi.org/10.1080/01495739.2016.1207118>.
- Kar, V.R., Mahapatra, T.R. and Panda, S.K. (2015), "Nonlinear flexural analysis of laminated composite flat panel under hygrothermo-mechanical loading", *Steel Compos. Struct.*, **19**(4), 1011-1033. <https://doi.org/10.12989/scs.2015.19.4.1011>.
- Kar, V.R., Panda, S.K. and Mahapatra, T.R. (2016), "Thermal buckling behaviour of shear deformable functionally graded single/doubly curved shell panel with TD and TID properties", *Adv. Mater. Res.*, **5**(4), 205. <https://doi.org/10.12989/amr.2016.5.4.205>.
- Karami, B., Shahsavari, D., Li, L., Karami, M. and Janghorban, M. (2018), "Thermal buckling of embedded sandwich piezoelectric nanoplates with functionally graded core by a nonlocal second-order shear deformation theory", *Proc. IMechE Part C: J. Mech. Eng. Sci.*, **10**, 1-15. <https://doi.org/10.1177/0954406218756451>.
- Kettaf, F.Z., Houari, M.S.A., Benguediab, M. and Tounsi, A. (2013), "Thermal buckling of functionally graded sandwich plates using a new hyperbolic shear displacement model", *Steel Compos. Struct.*, **15**(4), 399-423. <https://doi.org/10.12989/scs.2013.15.4.399>.
- Krommer, M., Vetyukov, Y. and Staudigl, E. (2016), "Nonlinear modelling and analysis of thin piezoelectric plates: Buckling and post-buckling behaviour", *Smart Struct. Syst.*, **18**(1), 155-181. <https://doi.org/10.12989/sss.2016.18.1.155>.
- Liew, K.M., Yang, J. and Kitipornchai, S. (2003), "Postbuckling of piezoelectric FGM plates subject to thermo-electro mechanical loading", *Int. J. Solid. Struct.*, **40**(15), 3869-3892. [https://doi.org/10.1016/S0020-7683\(03\)00096-9](https://doi.org/10.1016/S0020-7683(03)00096-9).
- Mirzavand, B. and Eslami, M.R. (2011), "A closed-form solution for thermal buckling of piezoelectric FGM rectangular plates with temperature-dependent properties", *Acta Mechanica*, **218**, 87-101. <https://doi.org/10.1007/s00707-010-0402-x>.
- Nami, M.R., Janghorban, M. and Damadam, M. (2015), "Thermal buckling analysis of functionally graded rectangular nanoplates based on nonlocal third-order shear deformation theory", *Aerosp. Sci. Technol.*, **41**, 7-15. <https://doi.org/10.1016/j.ast.2014.12.001>.
- Nazira, M., Eltahir, M.A., Mohamed, S.A. and Seddek, L.F. (2019), "Energy equivalent model in analysis of postbuckling of imperfect carbon nanotubes resting on nonlinear elastic foundation", *Struct. Eng. Mech.*, **70**(6), 737-750. <https://doi.org/10.12989/sem.2019.70.6.737>.
- Nguyen, T.K., Vo, T.P. and Thai, H.T. (2014), "Vibration and buckling analysis of functionally graded sandwich plates with improved transverse shear stiffness based on the first-order shear deformation theory", *Proc. IMechE Part C: J. Mech. Eng. Sci.*, **228**(12), 2110-2131. <https://doi.org/10.1177/0954406213516088>.
- Rathore, S.S. and Kar, V.R. (2023), "Thermoelastic eigenfrequency of pre-twisted FG-sandwich straight/curved blades with rotational effect", *Struct. Eng. Mech.*, **84**(4), 519-533. <https://doi.org/10.12989/sem.2023.86.4.519>.
- Reddy, J.N. (2004), *Mechanics of Laminated Composite Plates and Shells: Theory and Analysis*, 2nd Edition, CRC Press, Boca Raton, Florida.
- Rizov, V.I. (2021), "Delamination analysis of multilayered beams exhibiting creep under torsion", *Couple. Syst. Mech.*, **10**, 317-331. <https://doi.org/10.12989/csm.2021.10.4.317>.
- Wattanasakulpong, N. and Ungbhakorn, V. (2014), "Linear and nonlinear vibration analysis of elastically restrained ends FGM beams with porosities", *Aerosp. Sci. Technol.*, **32**(1), 111-120. <https://doi.org/10.1016/j.ast.2013.12.002>.
- Xiong, Q.L. and Tian, X. (2017), "Transient thermo-piezo-elastic responses of a functionally graded piezoelectric plate under thermal shock", *Steel Compos. Struct.*, **25**(2), 187-196. <https://doi.org/10.12989/scs.2017.25.2.187>.